Physics in Medicine & Biology

PAPER

Coded excitation for diverging wave cardiac imaging: a feasibility study

To cite this article: Feifei Zhao *et al* 2017 *Phys. Med. Biol.* **62** 1565

IOP Publishing | Institute of Physics and Engineering in Medicine Physics in Medicine & Biology

Phys. Med. Biol. **62** (2017) 1565–1584 doi:10.1088/1361-6560/aa58d7

Coded excitation for diverging wave cardiac imaging: a feasibility study

Feifei Zhao, Ling Tong, Qiong He and Jianwen Luo

Department of Biomedical Engineering, School of Medicine, Tsinghua University, Beijing 100084, People's Republic of China

E-mail: luo_jianwen@tsinghua.edu.cn

Received 2 September 2016, revised 30 December 2016
Accepted for publication 11 January 2017
Published 27 January 2017

Abstract

Diverging wave (DW) based cardiac imaging has gained increasing interest in recent years given its capacity to achieve ultrahigh frame rate. However, the signal-to-noise ratio (SNR), contrast, and penetration depth of the resulting B-mode images are typically low as DWs spread energy over a large region. Coded excitation is known to be capable of increasing the SNR and penetration for ultrasound imaging. The aim of this study was therefore to test the feasibility of applying coded excitation in DW imaging to improve the corresponding SNR, contrast and penetration depth. To this end, two types of codes, i.e. a linear frequency modulated chirp code and a set of complementary Golay codes were tested in three different DW imaging schemes, i.e. 1 angle DW transmit without compounding, 3 and 5 angles DW transmits with coherent compounding. The performances (SNR, contrast ratio (CR), contrast-to-noise ratio (CNR), and penetration) of different imaging schemes were investigated by means of simulations and *in vitro* experiments. As for benchmark, corresponding DW imaging schemes with regular pulsed excitation as well as the conventional focused imaging scheme were also included. The results showed that the SNR was improved by about 10 dB using coded excitation while the penetration depth was increased by 2.5 cm and 1.8 cm using chirp code and Golay codes, respectively. The CNR and CR gains varied with the depth for different DW schemes using coded excitations. Specifically, for non-compounded DW imaging schemes, the gain in the CR was about 5 dB and 3 dB while the gain in the CNR was about 4.5 dB and 3.5 dB at larger depths using chirp code and Golay codes, respectively. For compounded imaging schemes, using coded excitation, the gain in the penetration and contrast were relatively smaller compared to non-compounded ones. Overall, these findings indicated the feasibility of coded excitation in improving the image quality of DW imaging. Preliminary *in vivo* cardiac images of a healthy volunteer

were presented finally, and higher SNR and deeper penetration depth can be achieved by coded schemes.

Keywords: diverging wave, code excitation, chirp, golay, ultrasound, cardiac imaging

S Supplementary material for this article is available online

(Some figures may appear in colour only in the online journal)

1. Introduction

Ultrasound imaging is routinely used modality for cardiac imaging because it is safe, cost-effective, and most importantly it operates in real-time. The frame rates of most current commercial cardiac ultrasound systems are in the range of 25–40 Hz. Such frame rates are sufficient for anatomical visualization and rough kinematic evaluation (D'hooge *et al* 2000). However, they are too low to resolve some transient cardiac phases, e.g. isovolumetric contraction and isovolumetric relaxation phases. These transient phases may contain potentially important diagnostic information (Kanai 2009, Couade *et al* 2011, Papadacci *et al* 2013, Cikes *et al* 2014, Osmanski *et al* 2014, Grondin *et al* 2015). In addition, speeds of electromechanical waves (Pernot *et al* 2007, Kanai 2009) and shear wave (Pernot *et al* 2011) in the heart are in the range of 1–10 m s^{-1}. In order to capture these waves to assess the electromechanical and mechanical properties of myocardium, a much higher frame rate is required (Provost *et al* 2011, Tanter and Fink 2014).

To achieve ultra-high frame rate cardiac imaging, diverging wave (DW) imaging has gained increasing interest in recent years given its property of insonifying a large region within a single transmit (Hasegawa and Kanai 2011, Papadacci *et al* 2013). DW transmission can be obtained by placing a virtual source behind the transmit aperture. With a single DW transmit, the resulting image quality is significantly low in terms of signal-to-noise ratio (SNR), contrast and penetration. To improve the image quality, spatial coherent compounding of several DW transmits is typically adopted at the expense of decreasing the effective frame rate (Papadacci *et al* 2013, Tanter and Fink 2014). Papadacci and coworkers demonstrated that the compounding of 43 DWs transmits could offer grayscale images comparable to the conventional focused imaging using a line-by-line scan fashion (Papadacci *et al* 2013). However, the number of compounded DWs should keep small to avoid introducing significant motion artifacts particularly for motion estimation (Hergum *et al* 2007). The resulting image quality would thus be degraded as well. Nevertheless, the SNR, penetration and contrast remain low in DW imaging, which would hinder its further application in clinical practice.

Coded excitation can incorporate more energy in a transmission by increasing the excitation duration (Haider *et al* 1998, Chiao and Hao 2003, Wang *et al* 2003). In the past thirty years, this technique has been proposed for medical ultrasound imaging to improve the resulting SNR, penetration, and frame rate, etc (O'Donnell 1992, Misaridis and Jensen 2005a, 2005b, 2005c). Very recently, Song *et al* applied coded excitation in convex array based plane wave imaging (Song *et al* 2015). They demonstrated that coded excitation improved the SNR of ultrasound imaging and thus the detection of shear waves. Given their promising findings, the aim of this study was to further investigate the feasibility of using coded excitation in phased array based DW cardiac imaging to improve the resulting image quality, in particular the SNR and penetration.

The paper is organized as follows. The imaging schemes are designed to study the feasibility of coded excitation in DW imaging modes and the considered code waveforms are described briefly at first. Then the coded DW schemes are evaluated in simulations and phantom experiments to evaluate the gains in the SNR, contrast ratio (CR), contrast-to-noise ratio (CNR) and penetration depth. A healthy volunteer is involved for preliminary *in vivo* study. In the subsequent section, the corresponding results are presented. The discussions and conclusion are given in the end.

2. Methods

2.1. Imaging schemes setup

A standard 64 elements phased array transducer with a center frequency of 2 MHz, a pitch of 0.34 mm and a −6 dB bandwidth of 85% was used in this study. The element height was 13 mm and the kerf was 0.02 mm.

To investigate the performance of coded excitation in DW mode, the coded excitation DW coherent compounding schemes were compared with the non-coded DW coherent compounding schemes as well as the single line transmit (SLT) scheme, i.e. conventional focused imaging scheme.

Multiple steered DWs were transmitted for spatial coherent compounding, which is illustrated in figure 1. For non-steered DW, the virtual focal point was set to be 10 mm behind the probe surface to just cover all elements with a 90° scanning sector, while for steered DW, the virtual source was defined as the intersection point of the semi-circle (center: origin of coordinates, radius: 10 mm) and the corresponding steered line starting from the origin of coordinates (Hasegawa and Kanai 2011). Hasegawa *et al* (2011) used 15 DWs with steering angles in range of ±42°. As an empirical setting, the maximum steering angle $\theta_{\max}$ was set to be ±20° in our study considering the relatively large field of view and better image quality with compounding. Based on a previous study (Papadacci *et al* 2013), in order to minimize the motion artifact for myocardial velocity greater than 10 cm s^{-1} and imaging depth larger than 140 mm, the maximum number of compounding was limited to 5. So three setups, i.e. DW imaging without and with spatial coherent compounding of 3 or 5 angles, were used in this study. When compounding with 3 angles, the steering angles were set as −20°, 0° and 20°, while when compounding with 5 angles, the steering angles were set as −20°, −10°, 0°, 10°, and 20°, respectively.

For non-coded DW schemes, a short excitation pulse (figure 2(a)) consisting of 1.5 sinusoidal cycles at a central frequency of 2 MHz was used to generate the transmit patterns, while for coded excitation schemes, a pulse with a time-bandwidth product (TBP) greater than 1 was transmitted to achieve SNR and penetration gains.

Two representative types of code signals were analyzed in this study, i.e. linear frequency modulation (FM) signals (chirp) for frequency encoding and complementary binary codes (Golay codes) for phase encoding. Chirp signals are demonstrated to achieve the highest SNR gain in clinical evaluation, because it can increase both the pulse duration and sweeping bandwidth to fulfill a high TBP. On the other hand, Golay codes are easy to implement only relying on the phase modulation of transmission signal and are designed to perfectly eliminate the range lobes with two transmits (Misaridis and Jensen 2005a).

Generally, a temporal apodization is applied for chirp-based coded excitation to smooth the Fresnel ripples to lower the range lobes of the resulting compressed waveform (Misaridis and Jensen 2005a), and chirp with the temporal apodization is called tapered linear FM signals. In this study, a 20 μs linear FM chirp with a bandwidth of 3.6 MHz was assumed and

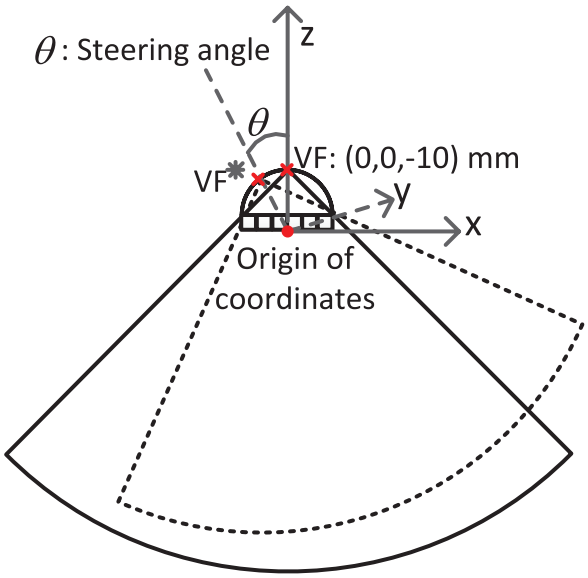

Figure 1. Principle of steered DW for spatial coherent compounding, VF and VF* stand for the virtual sources for non-steered and steered DW transmissions, respectively, where θ defines the steering angle.

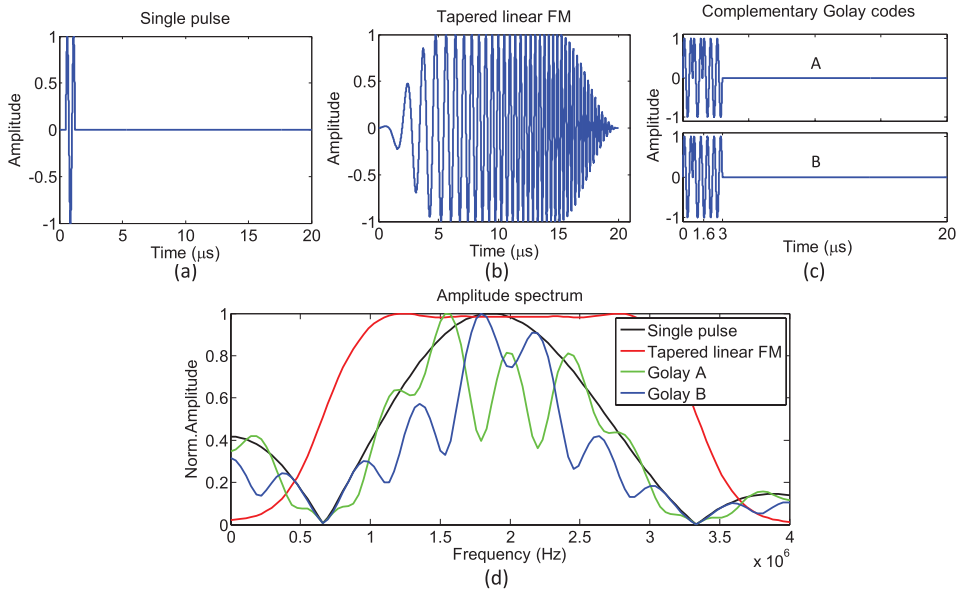

Figure 2. The code waveforms considered in this study and their frequency spectrums. (a) Single pulse, (b) tapered linear FM, (c) complementary Golay codes and (d) the corresponding amplitude spectrums.

Table 1. Setup of the imaging schemes.

		Non-coded			Chirp-coded			Golay-coded		
	SLT	1DW	3DWs	5DWs	1DW	3DWs	5DWs	1DW	3DWs	5DWs
Number of transmits	180	1	3	5	1	3	5	2	6	10
Frame rate gain	1	180	60	36	180	60	36	90	30	18

Tukey window ($\alpha = 0.5$) was used for temporal apodization, as illustrated in figure 2(b). A 4 bit complementary Golay codes were used: Golay A = (1 1 1 − 1), Golay B = (1 1 − 1 1), as illustrated in figure 2(c). For all the coded schemes, matched filters were used to compress the long pulse. The corresponding frequency spectrums of these waveforms are also presented in figure 2(d).

Full aperture was used on both transmit and receive for each imaging scheme and the imaging sector was fixed at 90° For SLT, rectangular apodization was applied on transmit, and the transmitted focal depth was set to be 70 mm. For DW modes, Tukey window ($\alpha = 0.5$) was used on both transmit and receive. The full channel data were acquired at a sampling frequency of 50 MHz and subsequently beamformed to obtain 180 imaging lines using the typical delay-and-sum fashion. For each receive beams, dynamic focusing with an F-number of 2 was used. The resulting grayscales images were normalized by their own maximum levels.

The imaging modes involved in this study are summarized in table 1. Note that the number of transmits and the gain in frame rate of each scheme are indicated taking the conventional SLT mode as reference.

2.2. Simulations

The simulations were done in Field_II (Jensen 1996). The acoustic attenuation was not taken into account in the simulations. A 10 dB Gaussian white noise was added into the channel data before beamforming was performed. All the data post-processing of the simulations and experiments were performed in Matlab 2015 environment (The MathWorks, Inc., Natick, MA, USA).

2.2.1. Simulations of point spread function. Basing on the transducer configuration, the point spread function (PSF) was simulated. Five point scatterers were placed at different depths (30–110 mm) which were 20 mm apart from each other at the azimuthal center axis of the image. In order to test the feasibility of pulse compression in the DW mode, five point scatterers were imaged only using DW, chirp-coded DW and Golay-coded DW schemes, as well as SLT, respectively. DW coherent compounding was not included here.

2.2.2. Simulations of tissue phantom. According to the different imaging schemes listed in table 1, a tissue phantom was simulated to study the performances of coded excitation on B-mode images. Randomly generated scatterers with a density of 25 mm^{-3} in dimensions of $60 \times 4 \times 110\,mm^3$ (laterally × elevationally × axially) was considered. The tissue phantom included three cystic regions and three hyper-echoic regions at different depths (figure 6(a)). The scattering intensity of the hyper-echoic regions was set to be ten times higher than that in the background.

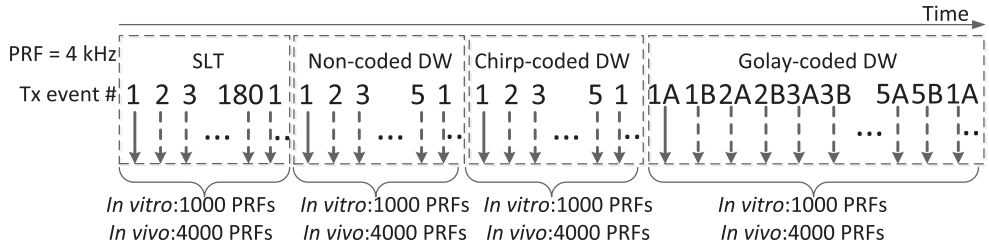

Figure 3. Sequences for experimental data acquisition. The acquisition time for each sequence is 0.25 and 1 s for the *in vitro* and *in vivo* experiments, respectively.

2.3. Experimental validation

To investigate the performances of coded excitation DW imaging *in vitro* and *in vivo*, the ultrasound advanced open platform (ULA-OP) (Tortoli *et al* 2009), an open platform characterized by high flexibility and wide access to raw data equipped with a phased array probe (PA230, Esaote SpA, Florence, Italy) was used. The transducer parameters were the same as those in the simulations. All images were acquired at the same output voltage level of 24 Vpp and with the same time gain compensation (TGC) of 7 dB cm^{-1}. In order to ensure the same imaging location and scanning views as far as possible for different modes in experimental conditions, especially for *in vivo* experiments, sequential sequences were used to obtain the data of different modes at once. The sequences are shown in figure 3. The first acquisition sequence was SLT, where 180 beams were transmitted to form one frame. It was followed by the non-coded DW sequence, which transmitted 5 DWs in 5 steered angles for DW coherent compounding. For the 1, 3 and 5 DWs compounding schemes considered in this study, 1, 3 and 5 DWs from the 5 transmissions were summed, respectively. The third sequence was chirp-coded DW, and the last one was Golay-coded DW.

2.3.1. In vitro experiments. A tissue mimicking phantom (CIRS Model 040GSE, Norfolk, VA, USA) with 0.5 dB/cm/MHz attenuation coefficient was used, and two views including several regions of interest (ROIs) were considered (figures 8 and 9). Moreover, the homogenous part of the tissue mimicking phantom was imaged using different schemes to quantify the penetration depth. The data acquisition for each sequence lasted for 0.25 s.

In order to test the feasibility of coded excitation when more DWs are compounded, different numbers of DWs compounding schemes (up to 17 DWs) with non-coded and chirp- or Golay-coded were performed on the tissue mimicking phantom.

2.3.2. In vivo experiments. A healthy male volunteer (heart rate: 65 beats per minute) was involved in the preliminary *in vivo* study. The apical four chamber view of the left ventricle was captured. The pulse repetition frequency was set to be 4 kHz with 90° FOV and 15 cm range. The data acquisition for each sequence lasted for 1 s. The electrocardiogram (ECG) data were acquired simultaneously to select the frames at the same cardiac phase in different modes for evaluations. This study was approved by the institutional review board of Tsinghua University and written informed consent was obtained from the subject.

2.4. Evaluations

2.4.1. Point spread function. To evaluate the axial and lateral beam widths, the range lobe and side lobe levels of coded excitation schemes in DW modes, the axial and lateral profiles of the PSF under noisy environments were extracted for all the point scatterers. Then the

beamwidth was quantified by measuring the main lobe width of the normalized PSF profile at −6 dB in the axial and lateral directions, respectively, which manifested the spatial resolution. The average side lobe level (ASLL) and average range lobe level (ARLL) (Weigang *et al* 2003, Karaman *et al* 2009) were also evaluated by averaging the normalized amplitudes of the side lobes and range lobes, as a prediction for contrast performances of different schemes on the corresponding tissue phantom images.

2.4.2. Tissue phantom simulations and experiments. To study the performance of tissue phantom simulations and experiments, the evaluation metrics included the SNR, CR, CNR and penetration depth. For the different numbers of DWs compounding schemes in experiments, the CR and CNR were quantified.

The SNR was defined as the ratio of signal power to noise power within an ROI based on the normalized envelope signals. In order to evaluate the noise power of the resulting images in simulations, firstly, the grayscale images were beamformed in noise-free environment for measurement of the signal power, then the noise power was evaluated from the power of the grayscale images in noisy environments subtracted by the signal power. In the experimental environment, the signal power and noise power were measured as follows (Shi *et al* 2003). Firstly, the images of the tissue mimicking phantom were captured; Secondly, the transmitters were turned off and images were captured in 'receive-only' mode. Thirdly, beamforming of both phantom images and receive-only images were performed with the same process. In the end, the SNR was calculated as the ratio of the signal power of the phantom images to the noise power of the receive-only images.

The CR was defined by the average cavity-to-background B-mode brightness difference, as:

$$\mathrm{CR} = \left|\mu_{\mathrm{cyst}} - \mu_{\mathrm{bck}}\right| \tag{1}$$

The CNR was defined as:

$$\mathrm{CNR} = \frac{\mathrm{CR}}{\sqrt{\sigma_{\mathrm{cyst}}^2 + \sigma_{\mathrm{bck}}^2}} \tag{2}$$

where μ_{cyst} and μ_{bck} are the mean amplitude levels in the cyst and background, σ_{cyst} and σ_{bck} are their standard deviations (Tong *et al* 2012), respectively.

To quantify the penetration depth in experiments, the average backscattered signals from the homogenous part of the tissue mimicking phantom were examined as a function of depth (figure 11). The curves show that the backscatter signals decrease with the depth until they reach a plateau at a specific depth where the power of the signal is equal to that of the noise. The specific depth was used to quantify the penetration depth (Mamou *et al* 2008).

2.4.3. In vivo experiments. For quantitative evaluation for *in vivo* experiments, the SNRs in two manually defined ROIs were calculated. These two ROIs were positioned in the myocardium at different depths (figure 14(a)). Both ROIs were square in shape ($5 \times 5\,\mathrm{mm}^2$) and manually tracked over different frames in order to stay in the same anatomical position. The cine-loops of a complete heart cycle for different schemes are shown as supplementary materials (stacks.iop.org/PMB/62/1565/mmedia).

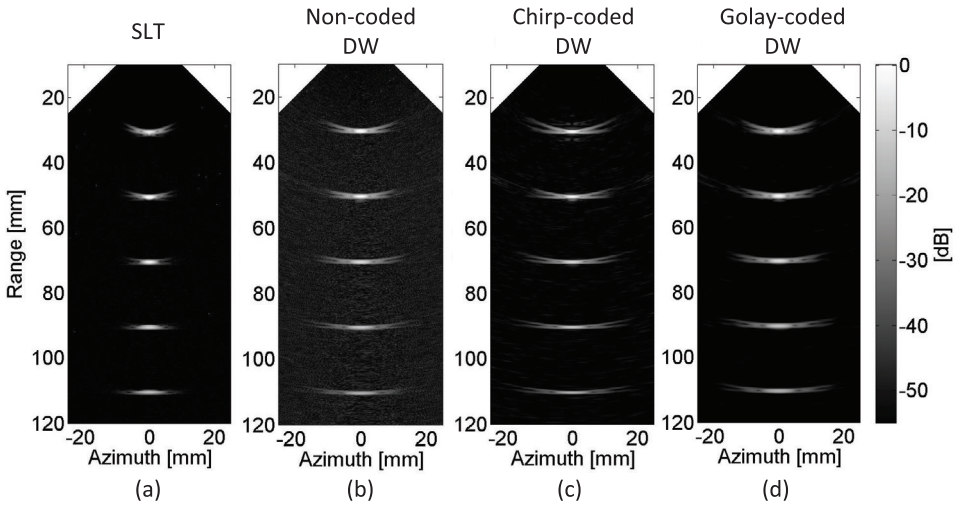

Figure 4. The PSFs of the four imaging schemes. (a) SLT, (b) DW, (c) chirp-coded DW, and (d) Golay-coded DW. The display dynamic range is 55 dB.

3. Results

3.1. Point spread function

The PSFs of the different imaging schemes are shown in figure 4. The noise reduction in the background due to coded excitation can be observed in the images. As expected, the lateral resolution of DW imaging scheme is lower than that of SLT. Coded schemes achieve comparable lateral resolution compared with non-coded scheme in DW imaging mode. Visually, the axial resolution of DW scheme is improved by using chirp coded excitation, but becomes worse when using Golay-coded excitation. In fact, the axial resolution is inversely proportional to the pulse bandwidth (Misaridis and Jensen 2005b). Chirp signals have the widest bandwidth (figure 2(d)), thus the axial resolution of chirp-coded PSF is optimized. Golay codes have narrower bandwidth (figure 2(d)) compared with single pulse signals, so the axial resolution is reduced in Golay-coded schemes. These results are quantified and shown in figures 5(e) and (f), which present the beam widths in the axial and lateral directions, respectively, for different schemes at different depths.

Figures 5(a) and 5(b) show the axial and lateral profiles of the point scatterer at the depth of 70 mm in the noise-free environment. The profiles are similar for non-coded and coded excitation DW schemes. In the noisy environment (figures 5(c) and (d)), coded excitation schemes show lower lobes level compared with non-coded scheme, therefore, they can suppress more noise and achieve higher SNR. To quantify the lobes level of the PSFs, figures 5(g) and (h) present the ARLL and ASLL of the PSF profiles in the noisy environment for different schemes at different depths. It is shown that coded excitation DW schemes perform better when compared with non-coded scheme, as coded excitation can suppress both the range lobes and side lobes (figures 5(c) and (d)). Chirp-coded scheme achieves an average range lobe decrease of 5 dB compared with non-coded scheme, while Golay-coded scheme achieves better ARLL, which is nearly comparable to the SLT mode (figure 5(g)). The quantitative values of the ASLL (figure 5(h)) confirm that the side lobe level in DW mode can be decreased to lower than -30 dB and -35 dB when using chirp- and Golay-coded excitation, respectively, while the side lobe level is over -30 dB for the point scatterers at deep depths when using non-coded excitation.

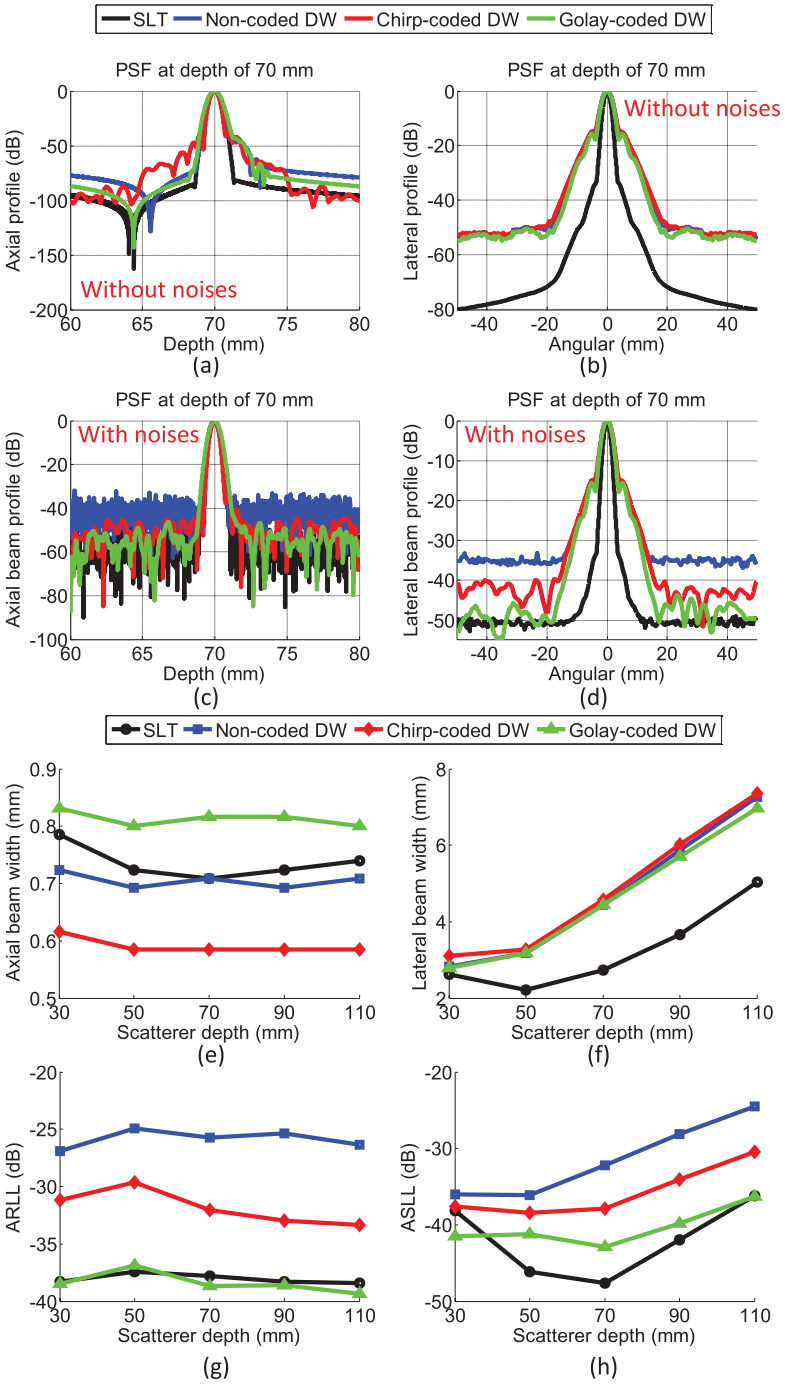

Figure 5. ((a) and (c)) Axial and ((b) and (d)) lateral beam profiles of the point scatterer at the depth of 70 mm for different schemes in noise-free and noisy environments, respectively. Quantitative characteristics of the PSFs including (e) axial beam width, (f) lateral beam width, (g) ARLL and (h) ASLL of SLT, DW, chirp-coded DW and Golay-coded DW schemes.

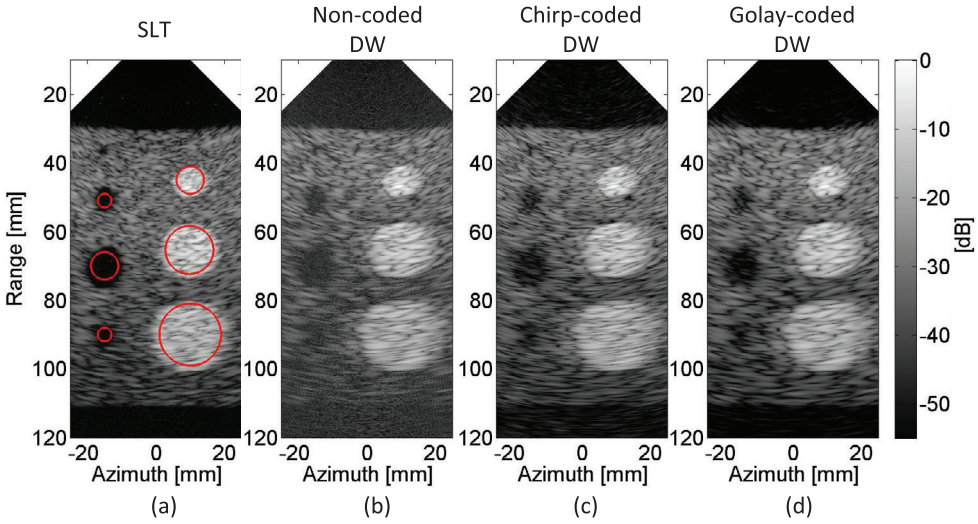

Figure 6. B-mode images of the simulated tissue phantom obtained by the four imaging schemes. (a) SLT, (b) DW, (c) chirp-coded DW, (d) Golay-coded DW. The display dynamic range is 55 dB. The ROIs used for quantitative analysis are indicated in (a).

3.2. Tissue phantom simulations

Figure 6 shows the B-mode images of the simulated tissue phantom obtained from different modes. Chirp- and Golay-coded DW schemes could suppress noise effectively compared with DW scheme, especially in the cystic regions.

To quantitatively analyze the performance of coded excitation in the phantom simulation environment, figure 7 shows the values of the SNR, CR and CNR in different ROIs (indicated in figure 6(a)). The corresponding values for SLT mode is indicated by the black horizontal line in each plot as a reference (applied also for phantom experimental and *in vivo* results).

For the SNR performance, Golay-coded schemes perform better than chirp-coded schemes with a gain of 11 dB, chirp-coded schemes achieve a gain of 6 dB for all the ROIs. For the CR performance, Golay-coded DW imaging is more robust than chirp-coded DW imaging. For the bottom cyst, the CR gain is about 5.5 dB and 7 dB for chirp and Golay-coded schemes, respectively, when using 1 or 3 DWs compounded, while a CR gain of ~3.5 dB and ~5 dB is obtained in 5 DWs compounding schemes for chirp- and Golay-based coded excitation, respectively. For the top cyst and medial cyst, the CR gain is slightly lower, which is about 2–4 dB and 3–5 dB for chirp and Golay-coded schemes, respectively. For the CNR performance, chirp and Golay-coded schemes obtain similar gain of ~4 dB in the bottom cyst, ~3 dB in the medial cyst and ~2 dB in the top cyst, respectively.

The CR and CNR gains are more significant at larger depths, while the SNR gain is almost the same for the ROIs at different depths. For the CR and CNR performances, the improvement of 3 or 5 DWs compounding schemes is slightly less than that of 1 DW mode, while the SNR gain is almost the same for one DW or multiple DWs coherent compounding modes.

3.3. In vitro experiments

Figures 8 and 9 shows the B-mode images of the phantom using different imaging schemes in two views. Brighter echo signals and higher cystic contrasts are achieved in coded schemes,

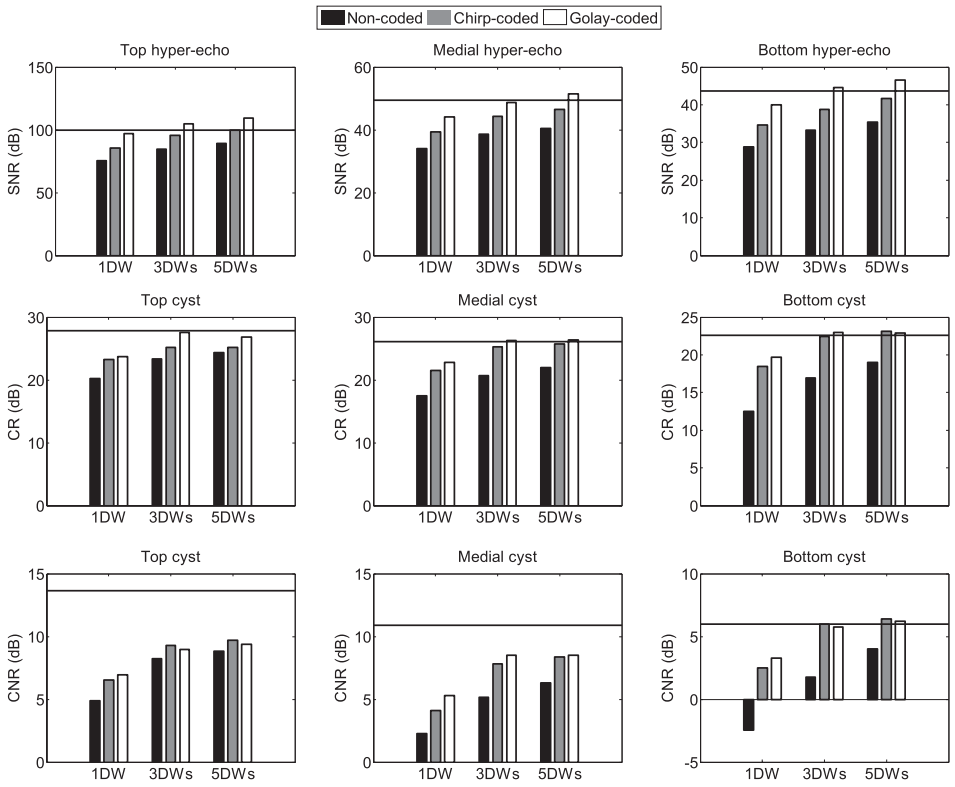

Figure 7. Quantitative analysis of tissue phantom simulations in different schemes, including the SNR, CR and CNR for different ROIs (indicated in figure 6(a)).

especially at larger depths. In figure 9, the deeper cystic region is hardly distinguished in non-coded DW mode, while for coded excitation DW modes, it can be well observed.

To quantitatively analyze the performance of the coded excitation DW schemes in the phantom experiments, figure 10 presents the SNR, CR and CNR performances in different modes including SLT, non-coded DW, chirp-coded DW and Golay-coded DW schemes.

For the SNR quantification, ROIs 1, 2 and 3 were considered involving regions at different depths and with different brightness. When using coded excitation, a gain of 10 dB is achieved for all the ROIs, Golay-coded schemes perform similarly to chirp-coded schemes except for ROI 2 when Golay-coded schemes with 3 or 5 DWs compounding are used. The advantages of Golay-coded schemes are not as evident as in the simulations.

ROIs 4 and 5 were involved for contrast quantification. The CR gain is about 6 dB and 4 dB for ROI 5 when chirp- and Golay-based coded excitation are used. At shallower depths, i.e. in ROI 4, coded excitation DW scheme has limited superiority, and the gain in the CR is ~1.5 dB and ~1 dB for chirp and Golay-coded schemes, respectively. For the CNR performance, chirp-coded schemes perform better than Golay-coded schemes. The gain is ~4.5 dB and ~3.5 dB for ROI 5, and ~1 dB and ~0.3 dB for ROI 4, using chirp- and Golay-coded schemes, respectively. Consistent with results in simulations, by compounding more DWs, the CR and CNR gains are less.

To evaluate the penetration depth of different imaging schemes, the mean backscattered signal amplitude curves varied with the depth are shown in figure 11. The penetration

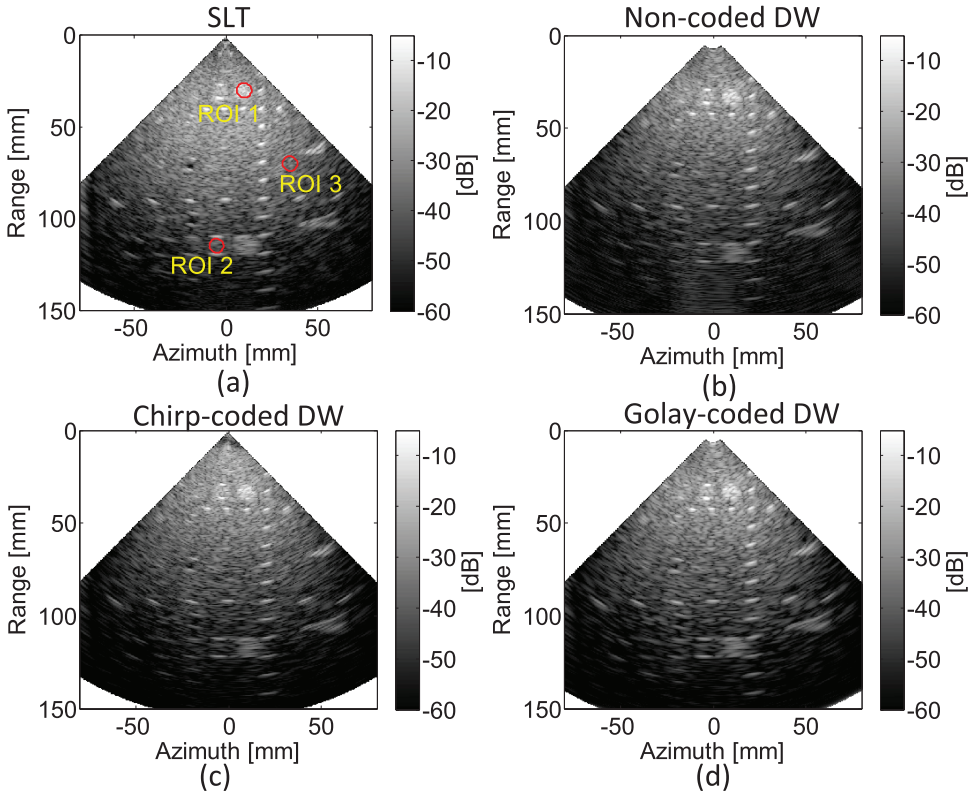

Figure 8. B-mode images of the phantom obtained by the four imaging schemes. (a) SLT, (b) DW, (c) chirp-coded DW, (d) Golay-coded DW. The display dynamic range is 55 dB. The ROIs used for quantitative analysis of the SNR, CR and CNR are indicated in (a).

depth is defined as the specific depth where the power of signal is equal to the power of noise, indicated by the arrows in figures 11(a) and (b) as examples. The penetration depth of non-coded 1DW is only 11.7 cm, while using coded excitation, the penetration depth can be increased by about 2 cm. For multiple DWs compounding schemes, coded excitation results in smaller penetration gain (figures 11(c)–(f)). To summarize, the penetration depth is increased by about 2–3 cm and 1–2 cm for chirp- and Golay-coded schemes, respectively, in 1 DW and coherent compounding of 3 DWs modes. For 5 DWs compounding schemes, the penetration gain was ~7 mm in coded schemes. The penetration depths of different imaging schemes are listed in table 2. The abbreviations of legends are the same as those in figure 11.

Figure 12 shows the quantitative contrast values in non-coded and chirp- or Golay- coded DWs compounding schemes with different numbers of compounding angles. The CR and CNR gains are about 2 dB when coded excitation applied. In addition, it shows that at the same contrast level indicated by the dark lines, the number of compounding angles in coded schemes is less than that in non-coded schemes.

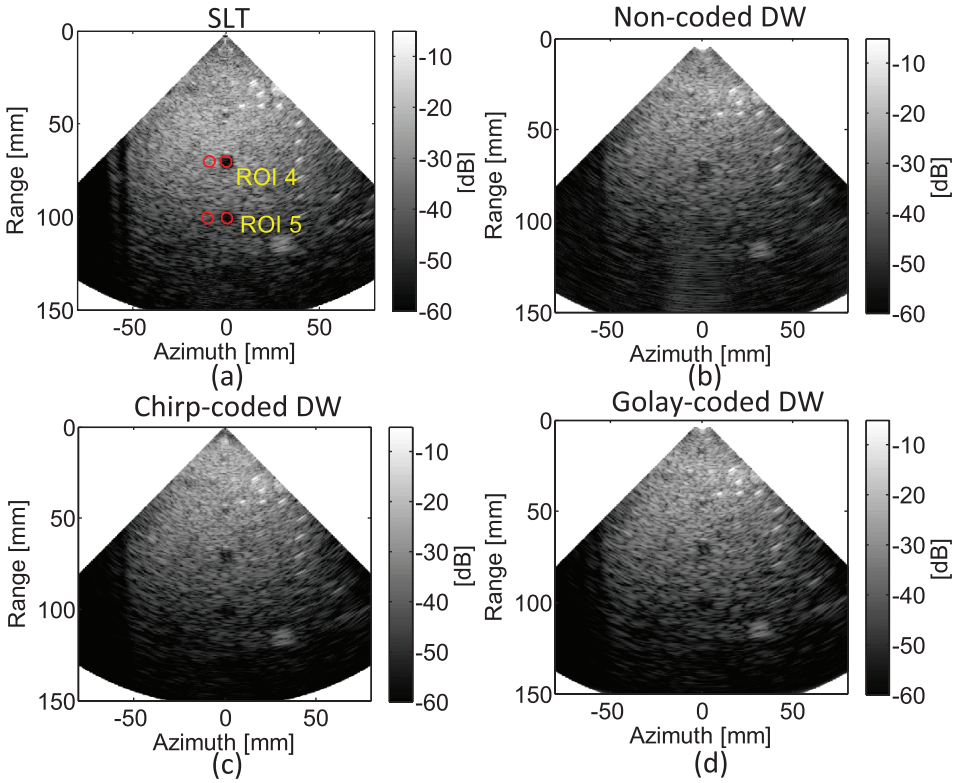

Figure 9. B-mode images of the phantom obtained by the four imaging schemes in another view. (a) SLT, (b) DW, (c) chirp-coded DW, (d) Golay-coded DW. The display dynamic range is 55 dB. The ROIs used for quantitative analysis of the SNR, CR and CNR are indicated in (a).

3.4. In vivo experiments

Figure 13 shows the *in vivo* B-mode images using different schemes. The brighter echo in the atrial region shows that coded excitation brings more energy into the tissue. The penetration depth for cardiac imaging is increased by using coded excitation, as indicated by the white arrows in figure 13.

Figure 14 shows the SNR performance of the *in vivo* images in different modes. Using coded excitation, a gain of about 10 dB is achieved for the SNR, chirp- and Golay-coded schemes perform comparably.

4. Discussion

Cardiac imaging using DW is gaining attention rapidly due to its high frame rate capability. Although spatial coherent compounding has been proposed to improve the quality of DW imaging, the relatively low penetration and SNR are still key problems to be solved. In this study, the feasibility of applying coded excitation to DW imaging for higher SNR, CR and CNR as well as deeper penetration depth was verified by means of simulations and *in vitro* experiments. For imaging in attenuated medium, chirp-coded schemes achieve more gains

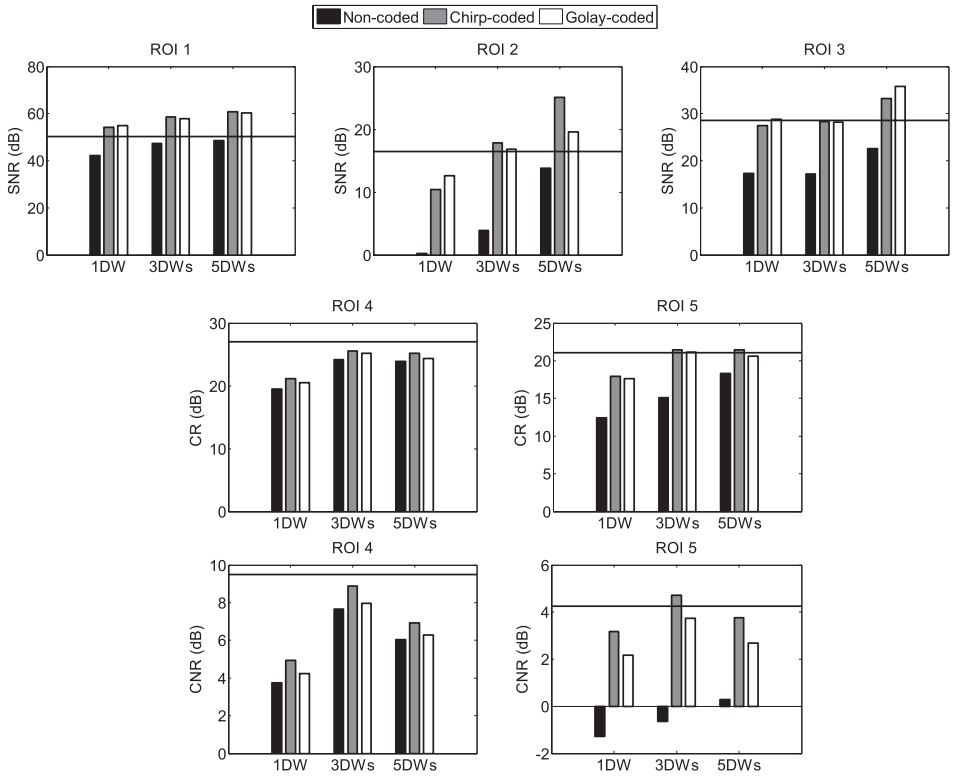

Figure 10. Quantitative analysis for the *in vitro* experiments using different schemes, including the SNR, CR and CNR for different ROIs (indicated in figure 9(a)).

than Golay-coded schemes. In the preliminary *in vivo* experiments, higher SNR and deeper penetration depth are achieved by using coded excitation.

The axial and lateral beam profiles in figures 5(c) and (d) show that in noisy simulation environment, coded excitation can suppress both the range lobes and side lobes, i.e. noise level, thus improving the image SNR and contrast. The quantitative values of ARLL and ASLL (figures 5(g) and (h)) show that Golay-coded scheme performs better than chirp-coded scheme in general with lower lobes level, because the complementary Golay codes are combined to eliminate the range lobes in simulations of static point scatterers without attenuation. In addition, more frames are compounded in Golay-coded scheme with complementary codes transmitted.

In the tissue phantom simulations, Golay-based coded excitation performs slightly better than chirp-based coded excitation (figure 7). The SNR gain of Golay-coded schemes is 4 dB higher than that of chirp-coded schemes. The CR gain of Golay-coded schemes is slightly higher than that of chirp-coded schemes in general. These results are in agreement with the PSF simulation results demonstrating that Golay-coded schemes have better ARLL and ASLL (figures 5(g) and (h)). For the CR and CNR performances, Golay- and chirp-coded schemes achieve different gains at different depths for the cystic regions (figure 7). These are in agreement with the ASLL results (figure 5(h)) as coded schemes optimize the lateral beam pattern when the wave diverges along the depth. The SNR, CR and CNR performances show that spatial coherent compounding also improves the image quality. It is notable that 3 DWs

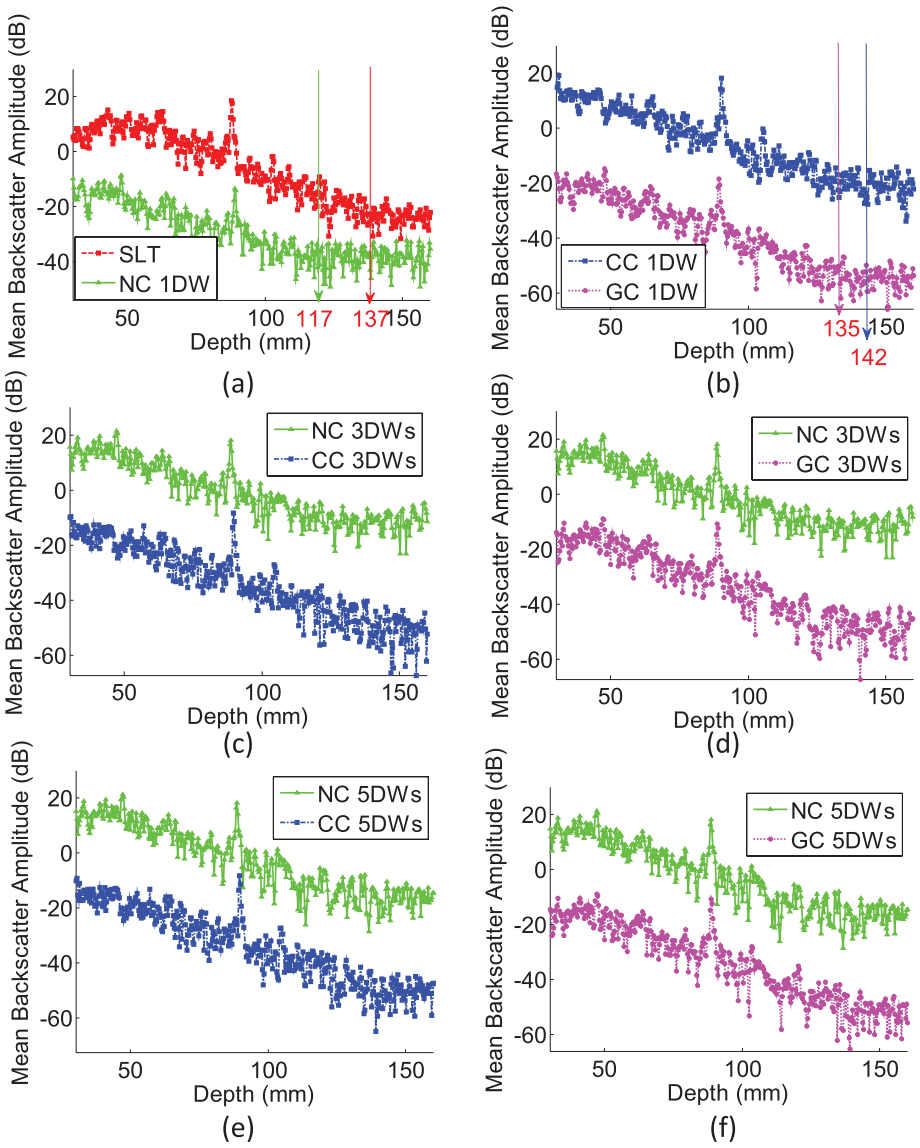

Figure 11. Mean backscattered signal amplitude as a function of depth using different schemes for quantitative analysis of the penetration depth. NC: non-coded; CC: chirp-coded; GC: Golay-coded; 1DW, 3DWs and 5DWs: one diverging wave, three diverging waves compounding and five diverging waves compounding.

Table 2. Penetration depths (cm) of different schemes.

SLT	NC 1DW	CC 1DW	GC 1DW	NC 3DWs	CC 3DWs	GC 3DWs	NC 5DWs	CC 5DWs	GC 5DWs
13.7	11.7	14.2	13.5	13	15	14.3	14.3	15	15

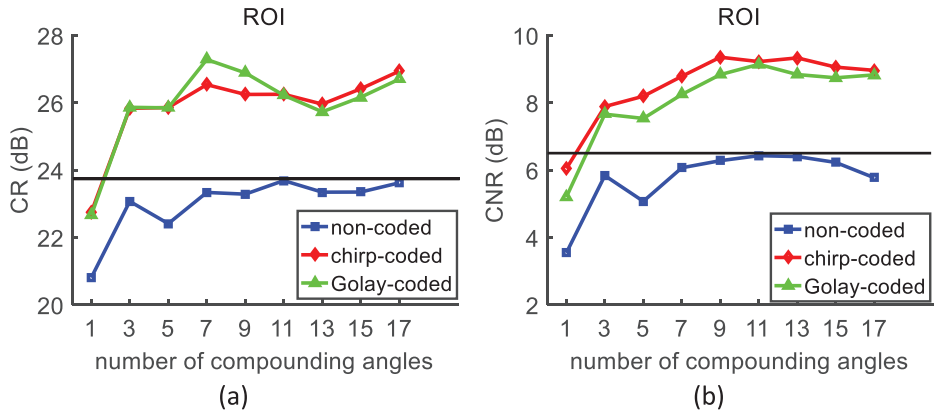

Figure 12. The CR(a) and CNR(b) quantification in the ROI based on different DW compounding schemes with or without coded excitation.

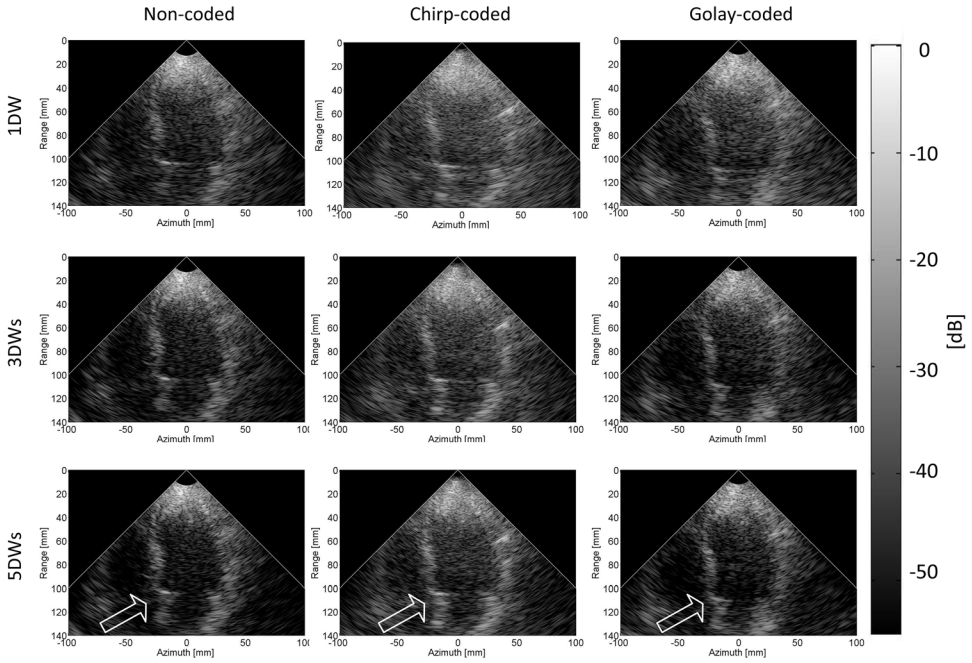

Figure 13. *In vivo* images of the left ventricle of the human subject in the apical four chamber view acquired from different imaging schemes, including non-coded DW, chirp-coded DW and Golay-coded DW schemes with 1, 3 and 5 DWs compounding, respectively.

compounding scheme with coded excitation can achieve higher SNR, CR and CNR compared with 5 DWs compounding scheme without coded excitation (figures 7 and 10), and the frame rate is higher at the same time (table 1). Therefore, by using coded excitation, the number of compounding angles in the DW imaging mode can be reduced for higher frame rate, without sacrificing the image quality.

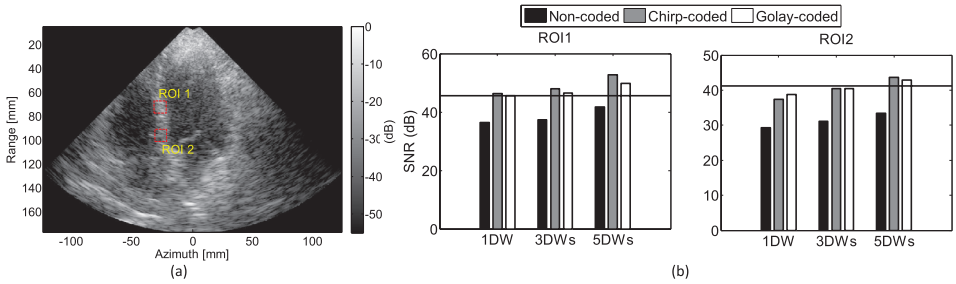

Figure 14. Quantitative values of the SNR of the ROIs in the septum for the *in vivo* images based on non-coded DW, chirp- and Golay-coded DW schemes, respectively. The ROIs are indicated in (a).

The *in vitro* experiments show that coded schemes obtain 10 dB gain in the SNR (figure 10). Chirp and Golay-coded schemes achieve similar SNR gain involving different ROIs. Moreover, the CR and CNR gains of Golay-coded schemes are slightly lower than those of chirp-coded schemes. These findings are inconsistent with the simulation results demonstrating that Golay-coded schemes achieve higher SNR, and higher CR gain as well as similar CNR gain compared with chirp-coded schemes, probably because there exists frequency shift due to attenuation in the experimental environment (Misaridis and Jensen 2005a). The frequency shift caused by attenuation lead to the incomplete elimination of range lobes in Golay-coded schemes.

The results reported in the literature based on conventional focused imaging mode demonstrate that Golay-based coded excitation outperforms chirp-based coded excitation for the SNR gain at shallower depth. While for imaging attenuated medium at depths of larger than 20 cm, Golay-based coded excitation performs worse due to the frequency shift (Misaridis and Jensen 2005a). But our *in vitro* experimental results show that, due to frequency shift, performances of Golay-coded schemes are reduced even in the near field, which is probably ascribed to the DW imaging mode. As for DWs, high side lobes and uneven energy distribution in the acoustic field are notable, the energy spreads and is weakened rapidly as the depth increases. Regarding to the penetration depth gain, chirp-coded DW scheme with higher TBP achieves 7 mm more than Golay-coded scheme (table 2). It is demonstrated that chirp-coded schemes outperform Golay-coded schemes when considering the combination of the SNR, CR, CNR and penetration depth quantification for the *in vitro* experiments (figures 9–11).

The acoustic attenuation is not included in the simulations given that the simulation program used, Field II, is based on linear acoustics theory. We have tried to quantify the results with attenuation added in one of our imaging schemes (i.e. chirp-coded 1DW) and found that it made no difference. So attenuation is not added in the simulations and the penetration depth is not quantified.

On the *in vivo* cardiac images, the contrast between myocardium and blood pools is degraded using coded schemes (figure 13). One possible reason is that, coded excitation passes high energy on both blood signals and myocardium signals, increasing the brightness of blood pool and myocardium in the images by different amount. The results show that Golay-coded schemes obtain higher contrast than chirp-coded schemes, because Golay-coded schemes have more frames to compound as a result of transmitting complementary codes (figure 3). Using coded excitation, chirp-coded schemes do not impact the frame rate, whereas Golay-coded schemes decrease the frame rate by a factor of 2 since two transmit events are intrinsically required to suppress the range lobes through pulse compression. However, for a pulse repetition frequency (PRF) of 5 kHz with non-compounded

DW, a compromise of a factor 2 in frame rate remains acceptable (frame rate = 2500 Hz) given the improved image quality as shown in figures 8–11. Furthermore, the contrast performance of more DWs compounding schemes with non-coded and chirp- or Golay-coded shown in figure 12 indicates that, to achieve the same image quality level (e.g. the level indicated by the dark line in figure 12), a less number of compounding angles is satisfied for coded schemes compared with that for non-coded schemes. That means that the number of compounding angles in coded DW schemes can be decreased to maintain higher frame rate. Hence, we believe that with coded excitation, it is possible to use a small number of compounds to obtain both high frame rate and acceptable image quality. Nevertheless, coded excitation DW imaging achieves higher SNR and penetration, which would be helpful for fast cardiac motion and intracardiac blood flow imaging. A comprehensive study of coded excitation DW imaging for cardiac function evaluation is the on-going work.

In experimental conditions, the variation of speed of sound in local tissues will affect the robustness of the delay-and-sum beamforming method and thus the image quality. However, the speed of sound and its variation are theoretically the same for different imaging schemes in our experiments, because they are mainly related to the physical properties of the tissues. In Misaridis and Jensen (2005a), a theoretical analysis revealed that the receiver output in coded schemes is related to the acoustic attenuation, but is independent of the speed of sound. Therefore, it is reasonable to assume that the variation of speed of sound has the same effect on the image quality involving non-coded or coded schemes. In conclusion, the variation of speed of sound theoretically will not affect the claimed findings in our experiments, i.e. the feasibility of coded excitation in DW imaging to obtain the SNR, contrast and penetration gain and their improved amount.

In figure 5(f), SLT has the highest lateral resolution (i.e. the smallest beamwidth) for the point scatterer at the depth of 50 mm, although the focal depth is at 70 mm. This is probably because of the relatively large length of focal zone (covering depths from 50 mm to 80 mm) due to the small aperture size (~20 mm) and low center frequency (~2 MHz) used in our experimental setup (Azhari 2010). In addition, for sector scanning based on phased array, the beamforming is performed in sector view with the same incremental angle, so the lateral sampling rate decreases along with the depth, resulting in a broader beam in deeper regions. In contrast, the ASLL values of the SLT mode (figure 5(h)) show that the point scatterer at the focal depth (70 mm) has the best beam pattern.

In figure 10 for ROI 4, the CNR in 5DWs compounding scheme is worse than that in 3DWs compounding scheme. The reason is that in DW transmit schemes, the PSF patterns are asymmetrical when virtual source with steering angle is used, and the asymmetry is different when using different steering angles. So different asymmetry based on different steering angles make it possible to increase the image quality using spatial compounding. However, this might also cause that the main lobe energy and side lobes energy of the PSF patterns are not increased proportionally when more steered DWs are compounded. In spite of this phenomenon, the image contrast shows a fluctuant ascending tendency with more compounding angles, as shown in figure 12. We can see that for both non-coded and coded schemes, the contrast performance generally increases with more compounding angles, although the increasing factor is not monotonous.

The limitation in this study is that only two types of codes were considered in this study, Chirp signals can increase both the duration time and sweeping bandwidth to achieve high TBP while maintaining the axial resolution, but chirps are more demanding as it relies on arbitrary waveform transmission, which may not be readily available in most ultrasound machines. Golay codes are easier to apply to clinical applications, but its applicability will be limited by the effects caused by the attenuation and motion of tissues.

To achieve high frame rate of cardiac imaging based on phased array, Cikes *et al* (2014) reviewed the potential methods including retrospective gating, multiline acquisition/transmit imaging and plane wave/DW imaging. We focus on plane wave and DW imaging for that they

can achieve ultrahigh frame rate relying on insonifying the whole region within a single transmit and parallel beamforming. Although Tong *et al* (2012) proved that plane wave outperforms DW particularly in far field for its unaffected wave pattern along the depth, for cardiac applications based on phased array, plane wave will be limited for its narrow field of view due to the narrow footprint of phased array and its small overlapped region with multiple steered plane waves for spatial coherent compounding. Plane wave imaging based on phased array cannot cover the entire heart because of insufficient scanning sector and depth (Papadacci *et al* 2013). So DW imaging is our research focus aiming to obtain very high frame rate. In addition, coded excitation has been proved to improve the SNR and penetration depth, so to help detecting the shear wave propagation based on plane wave imaging scheme (Song *et al* 2015). The objective of our study is applying the coded excitation to DW imaging to help solve the low SNR, contrast and penetration depth problems of DW imaging. The same principle is assumed to be applicable for other high frame rate imaging methods, and the details are not included here for it is beyond the scope of our aim.

Based on our finding, using coded excitation, not all these quality parameters are improved to a significant degree. For example, the penetration depth is mostly improved by 2.5 cm. However, even 2.5 cm in penetration depth gain is meaningful for cardiac applications, so that the apical 4 chamber view can be imaged more clearly for the more comprehensive assessment of the whole heart.

5. Conclusion

This study investigated the potential of coded excitation in high frame rate cardiac imaging using DW. The results of simulations and *in vitro* experiments demonstrated the feasibility of coded excitation DW for high frame rate imaging in attaining better SNR, CNR, CR and penetration depth compared to non-coded schemes. It was also found that chirp signals achieved better performance than Golay pulses. The preliminary *in vivo* study validated the SNR and penetration depth gain when coded excitation was applied.

Acknowledgments

This study was supported in part by the National Natural Science Foundation of China (61271131, 61322101, 81471665 and 81561168023), the National Key R&D Program of China (2016YFC0102201 and 2016YFC0104705), China Postdoctoral Science Foundation (2014M560094) and the Shenzhen Science and Technology Plan Project (JCYJ20140417115840275).

References

Azhari H 2010 *Basics of Biomedical Ultrasound for Engineers* (New York: Wiley)

Chiao R Y and Hao X 2003 Coded excitation for diagnostic ultrasound: a system developer's perspective *Proc. IEEE Ultrason. Symp. (IUS)* pp 437–48

Cikes M, Tong L, Sutherland G R and D'hooge J 2014 Ultrafast cardiac ultrasound imaging: technical principles, applications, and clinical benefits *JACC: Cardiovasc. Imaging* **7** 812–23

Couade M, Pernot M, Messas E, Bel A, Ba M, Hagège A, Fink M and Tanter M 2011 *In vivo* quantitative mapping of myocardial stiffening and transmural anisotropy during the cardiac cycle *IEEE Trans. Med. Imaging* **30** 295–305

D'hooge J, Heimdal A, Jamal F, Kukulski T, Bijnens B, Rademakers F, Hatle L, Suetens P and Sutherland G R 2000 Regional strain and strain rate measurements by cardiac ultrasound: principles, implementation and limitations *Eur. J. Echocardiogr.* **1** 154–70

Grondin J, Wan E, Gambhir A, Garan H and Konofagou E 2015 Intracardiac myocardial elastography in canines and humans *in vivo IEEE Trans. Ultrason. Ferroelectr. Freq. Control* **62** 337–49

Haider B, Lewin P A and Thomenius K E 1998 Pulse elongation and deconvolution filtering for medical ultrasonic imaging *IEEE Trans. Ultrason. Ferroelectr. Freq. Control* **45** 98–113

Hasegawa H and Kanai H 2011 High-frame-rate echocardiography using diverging transmit beams and parallel receive beamforming *J. Med. Ultrason.* **38** 129–40

Hergum T, Bjastad T, Kristoffersen K and Torp H 2007 Parallel beamforming using synthetic transmit beams *IEEE Trans. Ultrason. Ferroelectr. Freq. Control* **54** 271–80

Jensen J A 1996 Field: a program for simulating ultrasound systems *Med. Biol. Eng. Comput.* **34** 351–3

Kanai H 2009 Propagation of vibration caused by electrical excitation in the normal human heart *Ultrasound Med. Biol.* **35** 936–48

Karaman M, Wygant I O, Oralkan O and Khuri-Yakub B T 2009 Minimally redundant 2D array designs for 3D medical ultrasound imaging *IEEE Trans. Med. Imaging* **28** 1051–61

Mamou J, Ketterling J A and Silverman R H 2008 Chirp-coded excitation imaging with a high-frequency ultrasound annular array *IEEE Trans. Ultrason. Ferroelectr. Freq. Control* **55** 508–13

Misaridis T and Jensen J A 2005a Use of modulated excitation signals in medical ultrasound. Part I: Basic concepts and expected benefits *IEEE Trans. Ultrason. Ferroelectr. Freq. Control* **52** 177–91

Misaridis T and Jensen J A 2005b Use of modulated excitation signals in medical ultrasound. Part II: design and performance for medical imaging applications *IEEE Trans. Ultrason. Ferroelectr. Freq. Control* **52** 192–207

Misaridis T and Jensen J A 2005c Use of modulated excitation signals in medical ultrasound. Part III: high frame rate imaging *IEEE Trans. Ultrason. Ferroelectr. Freq. Control* **52** 208–19

O'Donnell M 1992 Coded excitation system for improving the penetration of real-time phased-array imaging systems *IEEE Trans. Ultrason. Ferroelectr. Freq. Control* **39** 341–51

Osmanski B F, Maresca D, Messas E, Tanter M and Pernot M 2014 Transthoracic ultrafast Doppler imaging of human left ventricular hemodynamic function *IEEE Trans. Ultrason. Ferroelectr. Freq. Control* **61** 1268–75

Papadacci C, Pernot M, Couade M, Fink M and Tanter M 2013 High-contrast ultrafast imaging of the heart *IEEE Trans. Ultrason. Ferroelectr. Freq. Control* **61** 288–301

Pernot M, Couade M, Mateo P, Crozatier B, Fischmeister R and Tanter M 2011 Real-time assessment of myocardial contractility using shear wave imaging *J. Am. Coll. Cardiol.* **58** 65–72

Pernot M, Fujikura K, Fung-Kee-Fung S D and Konofagou E E 2007 ECG-gated, mechanical and electromechanical wave imaging of cardiovascular tissues *in vivo Ultrasound Med. Biol.* **33** 1075–85

Provost J, Nguyen V T, Legrand D, Okrasinski S, Costet A, Gambhir A, Garan H and Konofagou E E 2011 Electromechanical wave imaging for arrhythmias *Phys. Med. Biol.* **56** L1–11

Shi H, Al-Sadah J, Mackie T and Zagzebski J 2003 Signal to noise ratio estimates of ultrasound depth of penetration *Med. Phys.* **30** 1367

Song P, Urban M W, Manduca A, Greenleaf J F and Chen S 2015 Coded excitation plane wave imaging for shear wave motion detection *IEEE Trans. Ultrason. Ferroelectr. Freq. Control* **62** 1356–72

Tanter M and Fink M 2014 Ultrafast imaging in biomedical ultrasound *IEEE Trans. Ultrason. Ferroelectr. Freq. Control* **61** 102–19

Tong L, Gao H, Choi H F and D'hooge J 2012 Comparison of conventional parallel beamforming with plane wave and diverging wave imaging for cardiac applications: a simulation study *IEEE Trans. Ultrason. Ferroelectr. Freq. Control* **59** 1654–63

Tortoli P, Bassi L, Boni E, Dallai A, Guidi F and Ricci S 2009 ULA-OP: an advanced open platform for ultrasound research *IEEE Trans. Ultrason. Ferroelectr. Freq. Control* **56** 2207–16

Wang Y, Metzger K, Stephens D N, Williams G, Brownlie S and O'Donnell M 2003 Coded excitation with spectrum inversion (CEXSI) for ultrasound array imaging *IEEE Trans. Ultrason. Ferroelectr. Freq. Control* **50** 805–23

Weigang B, Moore G W, Gessert J, Phillips W H and Schafer M 2003 The methods and effects of transducer degradation on image quality and the clinical efficacy of diagnostic sonography *J. Diagn. Med. Sonogr.* **19** 3–13